Out-of-Plane Corrections for Autonomous Robotic Breast Ultrasound Acquisitions

M.K. Welleweerd[1], A.G. de Groot[1], V. Groenhuis[1], F.J. Siepel[1], S. Stramigioli[1,2]

Abstract— **Breast cancer affects one out of eight women. Ultrasound (US) plays an important role in the diagnostic workflow, especially during the biopsy phase, in which tissue is extracted from the lesion for further analysis. The extension from 2D to 3D US acquisitions has multiple benefits including enhanced lesion localization and improved registration with MRI data. Current commercial 3D US systems lack the ability to preserve the breast's original shape. Robotic US scanners follow tailored trajectories and produce high quality volumes by accurate localization of 2D slices captured with a conventional linear probe. Current methods require a patient specific model to plan the scanning trajectory.**

In this study we investigate how to change the direction of the scanning trajectory based on US feedback, such that no patient specific model is required to perform a scan. In our method, the scanning trajectory is kept tangent to the breast based on confidence maps of the US images and an estimation of current radius of curvature of the surface. We evaluated our approach on a realistic breast phantom. The robot revolves around the breast without prior knowledge of its shape. In ten scans, the RMS error between the probe's scanning plane and the breast's surface normal is 12.6° out-of-plane, and 4.3° in-plane. A 3D US reconstruction shows the acquired data. This is a step forward to fully autonomous, high quality robotic US volume acquisitions.

I. INTRODUCTION

One out of eight women is affected by breast cancer during her lifetime. Early detection of suspicious lesions is known to reduce the mortality rate [1]. Several imaging modalities play an important role in the detection and diagnosis of breast cancer such as mammography, ultrasound (US) and MRI.

The role of US in breast cancer diagnostics is versatile. If a lesion is found during an examination, a biopsy is required, which is a procedure in which some tissue from the abnormality is removed with a needle for further examination. A US guided biopsy is the preferred biopsy method, since this method gives real-time feedback, is straightforward, relatively cheap, fast and causes less patient discomfort compared to an MRI-guided biopsy. Additionally, US can play a role in detecting breast cancer in females with dense breasts [2].

However, US has some limitations as well. The sensitivity of US is low compared to e.g. MRI. Therefore, lesions detected on MRI may be difficult to detect on US. Additionally, B-mode US images represent 2D cross-sections of the tissue.

This, combined with the fact that the probe is manipulated manually, makes the interpretation of the spatial relation between imaged regions difficult, and screening the complete breast time consuming. Due to these limitations, a US guided biopsy may not be possible on an MR-detected lesion, and therefore an MR guided biopsy is necessary.

The extension of 2D US to 3D US images will partly solve these issues. A 3D US volume has multiple advantages over 2D US images: the interpretation of spatial relations between internal structures is independent of the radiologist's ability to interpret individual slices, the lesion size is measured more accurately, the reproduction of cross-sections at follow up studies is easier, and the registration of US data with MRI data is less complex due to more available features [3].

Therefore, a variety of solutions to produce 3D US volumes have been presented. A 3D US probe can be realized by integrating a motorized 1D array of transducer elements or extending to a 2D array of elements. These probes are suboptimal since the fabrication is complex and latency of the image generation combined with the unstable hand of the radiologist introduces errors [4]. Therefore, many systems work with regular linear probes, of which the motions are tracked through time and space. Examples of these are optically or electromagnetically tracked freehand techniques [5]. Furthermore, linear probes can be integrated on moving platforms to perform a reproducible tracked motion. Commercial breast volume scanners are available in supine and prone variations. Supine examinations cause significant deformation of the breast [6]. Examinations in prone position, such as US tomography, cause less deformation but the covered volume is limited and the system is not suitable for all breast shapes and sizes [7].

Theoretically, robots are ideal to perform 3D US acquisitions because they produce reproducible, precisely tracked motions. This results in evenly spaced US images and eases the volume reconstruction. Multiple degrees of freedom (DOFs) allow for complex trajectories adapted to the individual's breast shape and robots do not suffer from fatigue.

Usually, robotic US volume acquisitions consist of two steps: localization and scanning. The patient should be localized to plan the subsequent scanning phase. Currently employed methods are surface reconstruction based on stereo cameras [8] or a depth camera [6] and the registration of MRI data based on multi modality markers [9]. Patient-specific paths may be generated by projecting a generic path on a tesselated surface representing the patient [10].

Although the patient's position was determined during the localization phase, the pre-planned path may not perfectly
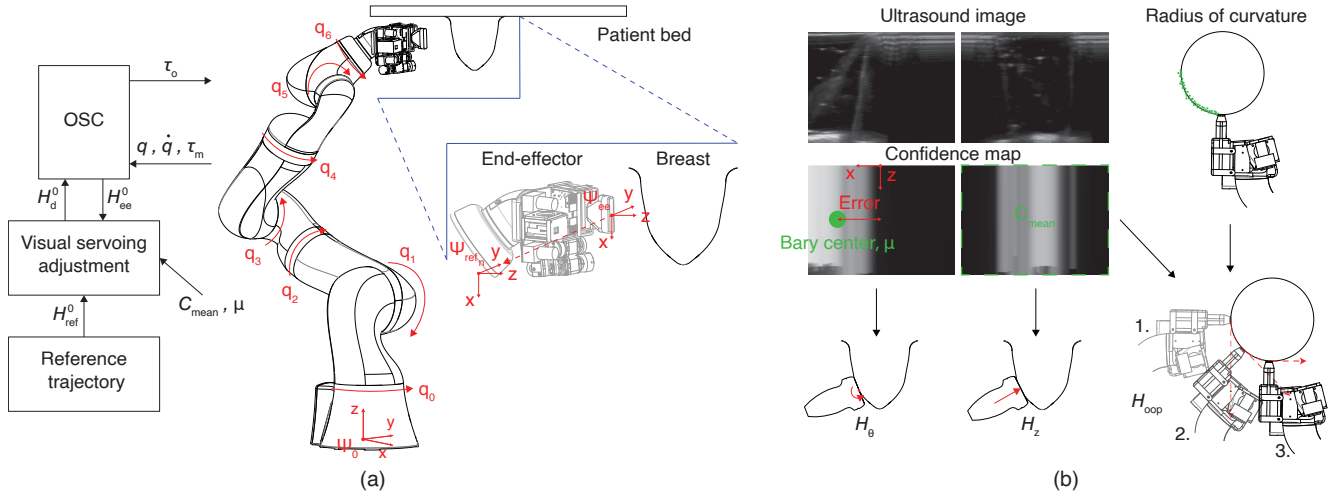
Fig. 1: A system overview. (a) A 7DOF manipulator with an end-effector is placed underneath the patient's breast. The reference trajectory is initially a straight line, but is wrapped around the breast in real-time based on the visual servoing algorithm. (b) Three probe adjustments can be performed based on US feedback and past EE positions. A rotation around the EE y-axis based on the bary center, a movement in the z-direction based on the mean confidence, or a rotation around the x-axis based on the current radius of curvature and the mean confidence.

follow the breast's shape. This can be due to inaccuracies in the surface reconstruction, or due to involuntary movements of the patient, such as breathing. There are several methods to compensate for inaccuracies of the pre-planned trajectory compared to the actual patient. Often, impedance control is utilized to account for small deviations and to ensure safe interactions between the robot, the patient and the radiologist [11]–[14]. However, to ensure good acoustic coupling of the US probe with the skin, some form of feedback during scanning is preferred. Sensing mechanisms currently employed in robotic scanning are force feedback and image feedback. Force feedback is mostly used to keep a constant pressure during scanning, but also to align the probe with the surface normal of the tissue [6], [14]–[18]. Kim et al. link the applied force to the image quality [19]. Our previous work showed that confidence maps are also an option to keep the US probe in contact with the tissue [10]. The advantage of image feedback over a constant normal force is the application of similar deformations for both softer and harder tissue. Additionally, confidence maps have been used to balance the probe contact with the tissue [10], [15], [17], [18]. Other visual servoing techniques, which connect end-effector (EE) behavior to image features are intensity based methods, feature tracking algorithms, image moments and speckle correlation or block matching [20]–[24].

In this paper we investigate how to utilize current and past US images to perform corrections on the path not only in-plane, like in our previous work [10], but also out of the US plane. The advantage is that the robot will find its way around the breast autonomously, and thus the localization step can be omitted. The out-of-plane corrections are achieved by keeping the confidence constant, and estimating the radius of curvature. The probe's scanning plane is kept perpendicular to the tangent plane of the surface and thus follows the breast's shape. The approach is validated by means of experiments on a realistic breast phantom.

II. THE SCANNING ALGORITHM

A. System overview

Fig. 1 shows an overview of the system. The patient lies in prone position on a bed with the examined breast through a hole such that it is freely accessible by the robot. The robot is placed underneath the bed, and is equipped with an EE carrying a US probe [9]. The robot's initial position coincides with the first pose and position of an initially planned trajectory. This trajectory is a straight line at a specified height in the negative y-direction of the EE frame, Ψ_{ee}. Once the scanning is started, the robot first localizes the breast surface. During scanning, the robot tries to keep the trajectory tangent to the surface based on the confidence of incoming US images (Fig. 1(b)). It does so by transforming the remaining part of the trajectory with the depicted transformations. The functioning of the various components is further elaborated in the following sections.

B. Operational space control

Operational space control, originally introduced by [25], is an approach to achieve desired EE behavior by applying virtual forces to the EE, and mapping these to the joint space of the robot. The control signal for the torques on the joints, $\boldsymbol{\tau}_c$, is expressed as

$$\boldsymbol{\tau}_c = \boldsymbol{J}^\mathsf{T}(\boldsymbol{q}) \, \boldsymbol{M}_x(\boldsymbol{q}) \left(\boldsymbol{k}_p \left(\boldsymbol{x}_d - \boldsymbol{x} \right) + \boldsymbol{k}_d \left(\dot{\boldsymbol{x}}_d - \dot{\boldsymbol{x}} \right) \right), \quad (1)$$

where $\boldsymbol{q}$ is the vector with joint positions, $\boldsymbol{J}^\mathsf{T}(\boldsymbol{q})$ is the Jacobian transpose, which maps the forces from the operational space to the joint space, $\boldsymbol{M}_x$ is the inertia matrix of the robot expressed in the operational space, which is

$$\boldsymbol{M}_x(\boldsymbol{q}) = \left(\boldsymbol{J}(\boldsymbol{q}) \, \boldsymbol{M}_q^{-1}(\boldsymbol{q}) \, \boldsymbol{J}^\mathsf{T}(\boldsymbol{q}) \right)^{-1}, \quad (2)$$

in which $\boldsymbol{M}_q(\boldsymbol{q})$ is the mass matrix of the robot expressed in joint space. $\boldsymbol{k}_p$ is the spring constant, $\boldsymbol{x}_d$ and $\dot{\boldsymbol{x}}_d$ are the desired position and velocity, respectively, $\boldsymbol{x}$ and $\dot{\boldsymbol{x}}$ are the current position and velocity in the operational space, respectively,

and k_d is the value of the damper. x_d is extracted from a homogeneous transformation matrix, H_d^0, which is generated by the visual servoing algorithm and describes the desired configuration of the EE-frame, Ψ_{ee}, with respect to the base frame, Ψ_0. In our work, the desired velocity, $\dot{x}_d$, is zero.

C. Confidence maps

Confidence maps were originally introduced by [26], to highlight attenuated regions of a US image. As such, they are useful to gain insight in the acoustic coupling of the probe with the skin. Each pixel (u, v) of an image is located in $\Omega := [1..n] \times [1..m]$. A confidence map $C : \Omega \to [0, 1]$ is a pixel-wise representation of the uncertainties in a US image $U : \Omega \to [0, 1]$. The map, $f : U \to C$, is based on the probability of a random walk starting from a pixel and reaching each of the virtual transducer elements. The random walk equilibrium meets three constraints: the top row of the US image has confidence 1, the bottom row has confidence 0, and the signal path is conform to US specific propagation constraints. In Fig. 1(b), examples of US images and their corresponding confidence maps are presented. Two features of the confidence maps are useful for adjustments of the pose and position of the probe: the mean confidence, C_{mean}, and the barycenter of the confidence, μ.

The mean confidence is a measure for the area of the transducer being in contact with the skin. It is defined as

$$C_{\text{mean}} = \frac{1}{n \cdot m} \sum_{(u,v) \in \Omega} C(u, v) . \tag{3}$$

If the mean confidence is controlled around a setpoint, C_s, a constant amount of contact with the skin is ensured. The confidence error is defined as: $e_c = C_s - C_{\text{mean}}$.

The barycenter of the confidence is defined as

$$\begin{aligned} \mu_u &= \frac{1}{C_\Omega} \sum_{(u,v) \in \Omega} u \cdot C(u, v), \\ \mu_v &= \frac{1}{C_\Omega} \sum_{(u,v) \in \Omega} v \cdot C(u, v), \end{aligned} \tag{4}$$

with $C_\Omega = \sum_{(u,v) \in \Omega} C(u, v)$ the total confidence. The pixel indices μ_u and μ_v correspond to EE coordinates μ_z and μ_x, respectively. A centered contact will result in $\mu_x = 0$. As in-plane rotations have an influence on the barycenter, the error is defined as $e_\mu = \arctan \frac{\mu_x}{\mu_z}$ radians.

Only the top of the confidence image is utilized in the control to make both features independent of the patient's physiology, as the first layer of tissue always consists of a skin and adipose layer.

D. Continuous contact

A controller is designed to maintain the mean confidence and the barycenter at the setpoints and as a result keep contact during a scan. Initially, the planned path is a straight line, its waypoints are listed in an array of transformation matrices, $H_{\text{ref}}^0(j)$, j indicating the current entry.

As outlined in Fig. 1(b), three types of transformations are applied to the initial trajectory: H_θ rotates the probe around
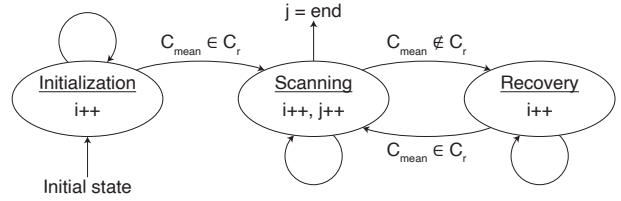

Fig. 2: The robot controller has three states: The initialization state, the scanning state and the recovery state. The initialization state ensures the initial contact. The scanning state takes new waypoints and continues the trajectory along the breast. The recovery state regains contact if the confidence is not sufficient.

its y-axis, H_z is adjusted to translate the waypoints towards or away from the breast, and the out-of-plane transformation, H_{oop}, is used to give the trajectory a new direction. The desired configuration of the EE in the i-th control iteration, $H_d^0(i)$, is defined as

$$H_d^0(i) = H_{\text{oop}}(i) \, H_{\text{ref}}^0(j) \, H_z(i) \, H_\theta(i) . \tag{5}$$

$H_\theta(i)$ is adjusted to maintain the confidence barycenter at its setpoint. This is performed by a PID controller, and the updated matrix is defined as:

$$H_\theta(i) = H_\theta(i-1) \begin{bmatrix} \text{Rot}_y(\theta) & \mathbf{0}^{3 \times 1} \\ \mathbf{0}^{1 \times 3} & 1 \end{bmatrix}, \tag{6}$$

in which $i - 1$ indicates the previous control iteration and $\text{Rot}_y(\theta)$ is a rotation matrix around the y-axis of θ radians.

A state machine is designed to apply modifications to $H_z(i)$ and $H_{\text{oop}}(i)$ in a coordinated manner (Fig. 2). It consists of three states: initialization, scanning and recovery.

1) Initialization state: This state ensures acoustic coupling between the breast surface and the US probe at the start of the scan. To achieve this, next to $H_\theta(i)$, $H_z(i)$ is manipulated by a PID controller. H_z is defined by

$$H_z(i) = H_z(i-1) \begin{bmatrix} \mathbf{I}^{3 \times 3} & d\,\hat{z} \\ \mathbf{0}^{1 \times 3} & 1 \end{bmatrix}, \tag{7}$$

in which I is the identity matrix, d is the displacement and $\hat{z}$ is the unity vector in the z-direction.

A mean confidence range, C_r, has been defined with the lower and upper boundary being $b_{\min}$ and $b_{\max}$, respectively, such that: $C_r = [b_{\min}, b_{\max}]$. The probe is in contact if $C_{\text{mean}} \in C_r$ and the controller moves on to the next state. In this state: $H_{\text{oop}} = I^{4 \times 4}$.

2) Scanning state: The robot moves along the path by incrementing j every control iteration. $H_{\text{oop}}(i)$ is adjusted to maintain the confidence setpoint: if the confidence is decreasing while performing a linear motion, the surface is expected to be convex, whereas an increasing confidence indicates a concave surface. As such, a PID controller can adjust the direction of the scan to maintain the confidence setpoint. Additionally, the radius of curvature of the surface is estimated by applying a Taubin circle fit on a window of the past trajectory and therefore, a prediction of the change in direction is available too [27].

The out-of-plane transformations perform a rotation around a frame defined by the orientation of the reference path and

the origin of the current EE position. The transformation is expressed in the base frame of the robot such that i-th out-of-plane rotation is defined as:

$$\boldsymbol{H}_{\mathrm{oop}}(i) = \boldsymbol{H}_{\mathrm{oop}}(i-1) \cdot$$
$$\begin{bmatrix} \boldsymbol{R}_{\mathrm{ref}}^0 & \boldsymbol{p}_{\mathrm{ee}}^0 \\ \boldsymbol{0}^{1\times3} & 1 \end{bmatrix} \begin{bmatrix} \mathrm{Rot}_x(\phi)^{3\times3} & \boldsymbol{0}^{3\times1} \\ \boldsymbol{0}^{1\times3} & 1 \end{bmatrix} \begin{bmatrix} \boldsymbol{R}_{\mathrm{ref}}^0 & \boldsymbol{p}_{\mathrm{ee}}^0 \\ \boldsymbol{0}^{1\times3} & 1 \end{bmatrix}^{-1}, \quad (8)$$

in which $\boldsymbol{R}_{\mathrm{ref}}^0$ is the orientation of the current reference waypoint, $\boldsymbol{p}_{\mathrm{ee}}^0$ is the current position of the EE and $\mathrm{Rot}_x(\phi)$ is a rotation around the x-axis by ϕ radians. In this state, $\boldsymbol{H}_z$ is kept constant. The controller goes to the recovery state if $C_{\mathrm{mean}} \notin C_{\mathrm{r}}$.

3) Recovery state: The controller adjusts $\boldsymbol{H}_z(i)$ to regain sufficient contact with the skin. Additionally, $\boldsymbol{H}_{\mathrm{oop}}(i)$ is adjusted such that the EE is again perpendicular to the newly estimated tangent. The controller moves back to the scanning state if $C_{\mathrm{mean}} \in C_{\mathrm{r}}$.

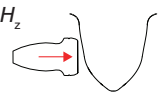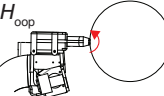Table I gives an overview of which manipulation is performed in which state of the state machine.
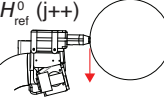
III. EXPERIMENTAL VALIDATION

A. Experimental setup

The setup (Fig. 3) consists of a seven DOFs robotic manipulator (KUKA Med 7 R800, KUKA GmbH, Germany) to which an EE is connected. The EE holds an L15-7L40H-5 linear US probe (Telemed UAB, Lithuania). The transformation of the transducer with respect to the flange is retrieved from the CAD design of the EE. The US probe is connected to a MicrUs EXT-1H (Telemed UAB, Lithuania) which streams the $27\times40\,\mathrm{mm}$ (w×h) US images with an update rate of $40\,\mathrm{Hz}$ to a workstation via a server. This workstation runs the algorithms and communicates with the manipulator via the fast research interface [28].

A breast phantom was made based on the surface reconstruction of a breast MRI of a woman laying in prone

TABLE I: Overview of the various manipulations to the current desired position and the corresponding states in which they are performed.

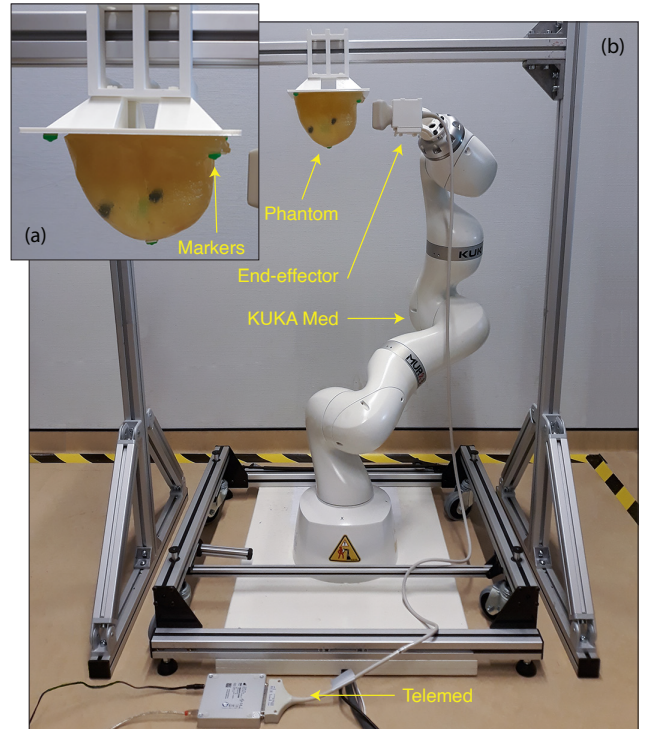| Control action	State		
	Initialization	Scanning	Recovery
H_z	✓		✓
H_θ	✓	✓	✓
H_{oop}		✓	✓
H_{ref}^0 (j++)		✓	

Fig. 3: The setup. (a) An enlarged version of the EE and the phantom with indicated the skin markers. (b) An overview of the setup with indicated: the KUKA MED medical robot, the EE, the phantom and the Telemed ultrasound machine.

position. Two molds were printed: an outer mold with the breast shape, and an inner mold. The inner mold was placed inside the outer mold to create a $5\,\mathrm{mm}$ thick skin layer which was filled with a PVCP/Plasticizer ($100\,\%\,/\,0\,\%$) mixture (Bricoleurre, France). Then, the inner mold was removed. The remaining volume was filled with a mixture of PVCP/Plasticizer ($100\,\%\,/\,0\,\%$) strands and PVCP/Plasticizer ($70\,\%\,/\,30\,\%$), to create a randomized structure resembling the adipose and glandular tissue in an actual breast. Silica powder was added to all mixtures in varying amounts (0-1 wt.%) to give the tissue varying degrees of echogenicity. The adipose tissue in this breast is up to ten times stiffer than actual adipose tissue, the skin layer has a stiffness comparable to actual skin [29]–[31].

Five skin markers were fabricated from PVCP mixed with green colorant (LUPA coloring, LureParts, The Netherlands). These were attached to a $1\,\mathrm{mm}$ PET disk and glued on the phantom. The markers are used for MRI data to robot registration during the experiment.

The breast was placed centered above the robot at a height of approximately $1.1\,\mathrm{m}$ (Fig. 3). This configuration resembles a patient laying in prone position on the bed.

B. Experiments

The fabricated phantom was scanned ten times. A scan contained the following steps: US gel was applied to the phantom with a brush. The EE was aligned with the first location of the path, $(x,y,z) = (0.06, 0, 1.01)\,\mathrm{m}$. The y- and z-axis of the EE were aligned with the -y and the x-
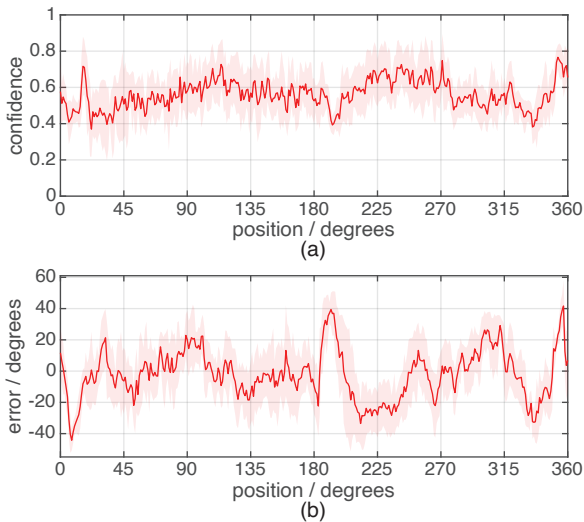
Fig. 4: (a) The average confidence, C_{mean} along the trajectory for ten scans. (b) The average error of the barycenter, e_μ, for ten scans. The opaque region indicates the standard deviation.
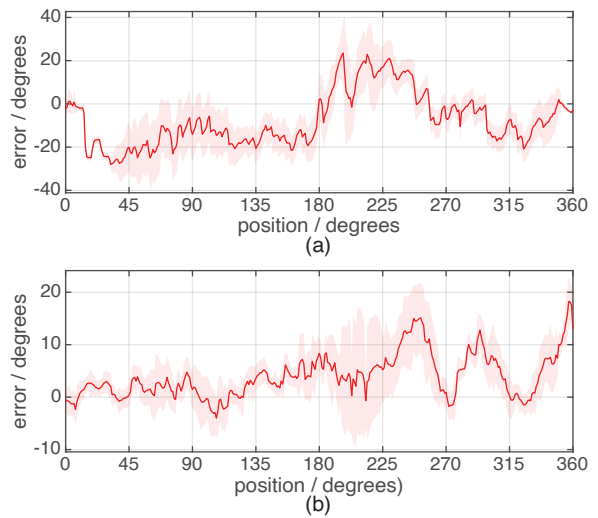

Fig. 5: (a) The average out-of-plane error of the probe with respect to the surface normal of the breast for ten scans. (b) The average in-plane error of the probe with respect to the surface normal of the breast for ten scans. The opaque region indicates the standard deviation.

axis of the base frame, respectively. The probe surface was located at $2\,\text{cm}$ from the breast surface in this position. The scan was started and the robot automatically navigated along the breast surface with a velocity of $2.5\,\text{mm}\,\text{s}^{-1}$. A scan was stopped when the robot had executed approximately $360°$ around the breast. The confidence setpoint, C_s, was 0.50. The confidence range in which the scanning state is active was $C_r = [0.35, 0.7]$. The boundaries were chosen asymmetric because a higher confidence is preferred over no contact. Additionally, a phantom-to-robot calibration was performed with stereo cameras to evaluate the quality of the US acquisitions afterwards.

C. Results

The robot succesfully revolved around the breast ten times. All plots are shown in polar coordinates with the breast at its center, because the trajectory approximates a circle.

In Fig. 4, the mean confidence and the error of the barycenter are plotted. The RMS error of the confidence was 0.08. The confidence is mostly above the setpoint of 0.5, because a too low confidence was penalized more by the controller than a too high confidence, due to the asymmetric boundaries that determine the robot state. The barycenter was on average $-2.2°$ off, whereas the RMS error is $12.2°$.

The EE's z-axis should be collinear with the breast's surface normal. To this end, the probe can rotate around the EE's x- and y-axis. We assessed the EE's orientation with respect to the phantom by means of the camera calibration and the surface reconstruction of the phantom. The out-of-plane error is defined as the angle between the breast's surface normal and the image plane. Thus, the rotation around the EE's x-axis necessary to align the image plane with the surface normal. The in-plane error indicates how much the rotation around the EE's y-axis is off. Fig. 5(a) and (b) present the out-of-plane and the in-plane error, respectively. On average, the out-of-plane error is $-7.6°$, and the RMS error $12.6°$. At

$0°$, the error builds up in the negative direction, because the robot did not record enough data to estimate the radius of curvature yet. Around $180°$, the error becomes positive, since the breast's cross section is ellipse shaped (see Fig. 6(a)), and the algorithm underestimates the radius of curvature on the flatter side. The mean in-plane error is $4.0°$, and the RMS error is $4.3°$. As expected, these numbers have the same order of magnitude as the errors in the barycenter.

Fig. 6(a) shows the robot trajectory with respect to the breast surface. It is shown that the breast is most indented around $0°$ and $210°$. This effect is also due to the algorithm's tendency to underestimate after a transition from a small to a large radius of curvature. Additionally, at $210°$, the EE's xy-plane is almost aligned with the world's xy-plane. The steep inclination of the breast's surface at this position makes that this plot is sensitive to calibration errors in this section.

Fig. 6(b) shows the confidence in the US images at $z = 1.01\,\text{m}$ for scan No. 9. The graph shows a confidence which is higher than the average confidence as shown in Fig. 4(a) in most sections. The confidence is usually the highest in the middle of an image. This cross section is approximately taken at the middle of all acquired images, and represents the highest confidence found for each location. From this image, it is clear that the breast volume is mostly covered with high confidence data. The confidence is lower in the middle, because the confidence decreases the further it travels through the phantom. There is a section in the middle which is not imaged and thus does not have confidence.

Fig. 6(c) shows the reconstructed US cross section. This reconstruction is based on the acquired US data, and a deformation compensation is applied based on the original shape as extracted from the MRI images of the phantom. Some features of the phantom are clearly distinguished, such as the $5\,\text{mm}$ thick skin layer.
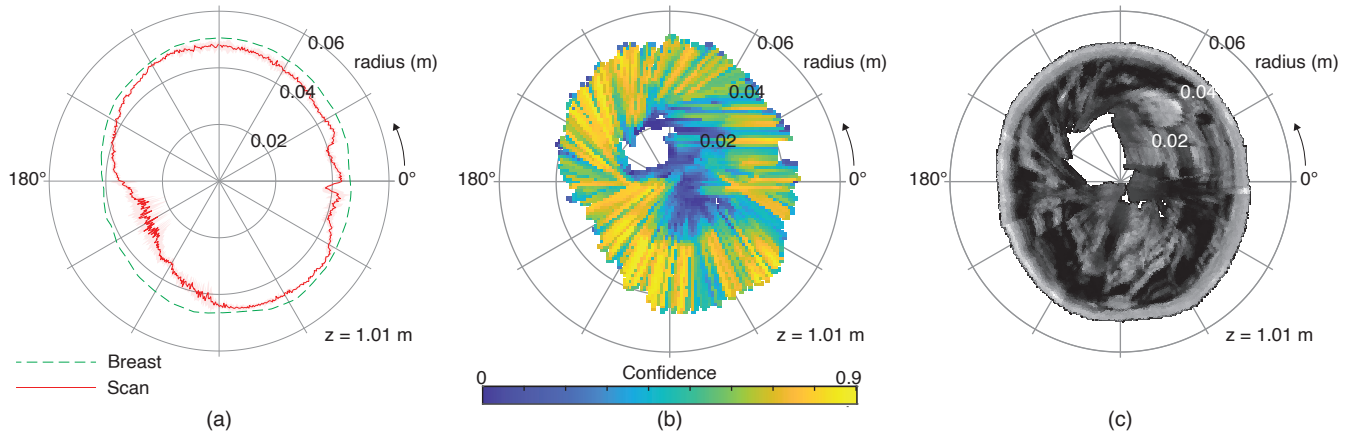
Fig. 6: (a) The anticipated cross-section (dashed) of the breast at height $z = 1.01\,\mathrm{m}$ and the the average US probe's position (solid) for ten scans. The opaque region indicates the standard deviation. (b) The confidence in the US signal in the cross-section of the breast at $z = 1.01\,\mathrm{m}$ for scan No. 9. This scan was the closest to the average trajectory shown in (a). (c) The generated US cross-section of the breast based on the acquired data during scan No. 9.

IV. DISCUSSION

This study presents an approach for fully automated robotic breast volume US acquisitions. The approach was tested in a realistic clinical setting with a breast phantom placed in prone position over the robot. The robot follows the breast surface without prior knowledge.

Our results show that it is feasible to control three DOFs of the EE based on confidence maps: a translation in the z-direction of the EE, an in-plane rotation and an out-of-plane rotation. This is an improvement over our previous study [10], which was able to control two degrees of freedom.

The addition of an extra DOF has a significant impact on the workflow of a robotic US acquisition. Other studies use some form of prerequisite information on which the US scan is based. Most often, this is a surface reconstruction of the scanned area, which can be acquired with stereo cameras [8], a depth camera [6], or registration with a MRI images [10]. Utilizing our implementation, the robot revolves around the breast based on just a generic initial path and US feedback. Calibration steps between the camera, the robot and the patient, the extra time taken by recording the surface data or the necessity of a pre-operative MRI are all ruled out, because the system depends on just the US data. Additionally, the complexity of the EE is reduced to just a linear US probe.

However, the US volume reconstruction becomes more complex if the preprocedural surface reconstruction is absent, because the initial state compared to the compressed state is unknown. In our study, we utilized the camera calibration and the surface reconstruction of the phantom for deformation compensation in the US volume reconstruction. We are investigating whether transitions from low to high confidence allow us to reconstruct the original breast shape during a scan. This allows not only the robotic acquisition, but also the reconstruction to be independent of prerequisite data.

Currently, the system's out-of-plane corrections still lag behind the actual surface normal of the breast. Consequently, Fig. 6(c) shows a section without data in the middle. The lag is caused by the system's dependence on a prediction of the radius of curvature, which is based on a past section of the

trajectory. Therefore, at the start of the scan, the prediction is not accurate yet, and later during the scan, if the radius of curvature transitions from small to large or vice versa too fast, the systems adapts with a delay. Position-wise this delay is less present, because the recovery state constantly reestablishes the contact of the probe with the skin.

The system's performance should be further examined under different circumstances. Currently, the system was tested on one phantom, with a specific size, shape and material. Although the phantom is a representative example, many variations occur in real life scenarios such as the quantity of US gel, actual human tissue and patient movements. The robustness may be improved by manually choosing the initial position of the probe, such that the initial configuration can be adapted to the breast's shape by e.g. an initial in-plane rotation. It is expected that differences in stiffness have minor impact on the results, since the adjustments are based on image-features, and not on force.

Currently, the acquisition time is approximately $180\,\mathrm{s}$, which is comparable to existing systems [7]. However, total volume coverage may require multiple sweeps at varying heights. Therefore, the scanning velocity and acquisition rate may have to be increased in future work.

Summarizing, the presented method shows potential for autonomous breast volume US acquisitions. The approach may also be applicable in other clinical settings such as skeletal muscle volume determination and abdomen screening.

V. CONCLUSION

This work investigates how to control three DOFs of the robot utilizing US feedback. The robot finds its way around a complex shape like the breast based on a simple reference trajectory and real-time US and position feedback. Currently, the RMS error of the in-plane and the out-of-plane alignment of the scanning plane with the surface normal is 4.3° and 12.6°, respectively. The acquired US data covers a significant part of the desired cross-section. The obtained results show the potential of the approach, which may also be interesting for other US scanning applications.

REFERENCES

[1] F. Bray, J. Ferlay, I. Soerjomataram, R. L. Siegel, L. A. Torre, and A. Jemal, "Global cancer statistics 2018: GLOBOCAN estimates of incidence and mortality worldwide for 36 cancers in 185 countries," *CA: A Cancer Journal for Clinicians*, vol. 68, no. 6, pp. 394–424, nov 2018.

[2] M. Nothacker, V. Duda, M. Hahn, M. Warm, F. Degenhardt, H. Madjar, S. Weinbrenner, and U.-S. Albert, "Early detection of breast cancer: benefits and risks of supplemental breast ultrasound in asymptomatic women with mammographically dense breast tissue. A systematic review," *BMC Cancer*, vol. 9, no. 1, p. 335, dec 2009.

[3] S. Liu, Y. Wang, X. Yang, B. Lei, L. Liu, S. X. Li, D. Ni, and T. Wang, "Deep Learning in Medical Ultrasound Analysis: A Review," *Engineering*, vol. 5, no. 2, pp. 261–275, 2019.

[4] Q. Huang and Z. Zeng, "A Review on Real-Time 3D Ultrasound Imaging Technology," *BioMed Research International*, vol. 2017, pp. 1–20, 2017.

[5] F. Mohamed and C. Vei Siang, "A Survey on 3D Ultrasound Reconstruction Techniques," in *Artificial Intelligence - Applications in Medicine and Biology*. IntechOpen, jul 2019, ch. 4.

[6] Q. Huang, B. Wu, J. Lan, and X. Li, "Fully Automatic Three-Dimensional Ultrasound Imaging Based on Conventional B-Scan," *IEEE Transactions on Biomedical Circuits and Systems*, vol. 12, no. 2, pp. 426–436, apr 2018.

[7] D. Amy, *Lobar Approach to Breast Ultrasound*, D. Amy, Ed. Cham: Springer International Publishing, 2018.

[8] T. E. Chemaly, F. J. Siepel, S. Rihana, V. Groenhuis, F. van der Heijden, and S. Stramigioli, "MRI and stereo vision surface reconstruction and fusion," in *2017 Fourth International Conference on Advances in Biomedical Engineering (ICABME)*, vol. 2017-Octob. IEEE, oct 2017, pp. 1–4.

[9] M. K. Welleweerd, F. J. Siepel, V. Groenhuis, J. Veltman, and S. Stramigioli, "Design of an end-effector for robot-assisted ultrasound-guided breast biopsies," *International Journal of Computer Assisted Radiology and Surgery*, vol. 15, no. 4, pp. 681–690, apr 2020.

[10] M. Welleweerd, A. de Groot, S. de Looijer, F. Siepel, and S. Stramigioli, "Automated robotic breast ultrasound acquisition using ultrasound feedback," in *2020 IEEE International Conference on Robotics and Automation (ICRA)*. IEEE, may 2020, pp. 9946–9952.

[11] C. Graumann, B. Fuerst, C. Hennersperger, F. Bork, and N. Navab, "Robotic ultrasound trajectory planning for volume of interest coverage," *Proceedings - IEEE International Conference on Robotics and Automation*, vol. 2016-June, pp. 736–741, 2016.

[12] R. Kojcev, B. Fuerst, O. Zettinig, J. Fotouhi, S. C. Lee, B. Frisch, R. Taylor, E. Sinibaldi, and N. Navab, "Dual-robot ultrasound-guided needle placement: closing the planning-imaging-action loop," *International Journal of Computer Assisted Radiology and Surgery*, vol. 11, no. 6, pp. 1173–1181, jun 2016.

[13] K. Mathiassen, J. E. Fjellin, K. Glette, P. K. Hol, and O. J. Elle, "An Ultrasound Robotic System Using the Commercial Robot UR5," *Frontiers in Robotics and AI*, vol. 3, no. February, pp. 1–16, 2016.

[14] Z. Jiang, M. Grimm, M. Zhou, Y. Hu, J. Esteban, and N. Navab, "Automatic Force-Based Probe Positioning for Precise Robotic Ultrasound Acquisition," *IEEE Transactions on Industrial Electronics*, vol. 0046, no. c, pp. 1–1, 2020.

[15] S. Virga, O. Zettinig, M. Esposito, K. Pfister, B. Frisch, T. Neff, N. Navab, and C. Hennersperger, "Automatic force-compliant robotic ultrasound screening of abdominal aortic aneurysms," in *2016 IEEE/RSJ International Conference on Intelligent Robots and Systems (IROS)*. IEEE, oct 2016, pp. 508–513.

[16] A. S. B. Mustafa, T. Ishii, Y. Matsunaga, R. Nakadate, H. Ishii, K. Ogawa, A. Saito, M. Sugawara, K. Niki, and A. Takanishi, "Development of robotic system for autonomous liver screening using ultrasound scanning device," *2013 IEEE International Conference on Robotics and Biomimetics, ROBIO 2013*, no. December, pp. 804–809, 2013.

[17] P. Chatelain, A. Krupa, and N. Navab, "Confidence-Driven Control of an Ultrasound Probe," *IEEE Transactions on Robotics*, vol. 33, no. 6, pp. 1410–1424, dec 2017.

[18] Z. Jiang, M. Grimm, M. Zhou, J. Esteban, W. Simson, G. Zahnd, and N. Navab, "Automatic Normal Positioning of Robotic Ultrasound Probe Based only on Confidence Map Optimization and Force Measurement," *IEEE Robotics and Automation Letters*, vol. 5, no. 2, pp. 1342–1349, 2020.

[19] Y. J. Kim, J. H. Seo, H. R. Kim, and K. G. Kim, "Development of a control algorithm for the ultrasound scanning robot (NCCUSR) using ultrasound image and force feedback," *The International Journal of Medical Robotics and Computer Assisted Surgery*, vol. 13, no. 2, p. e1756, jun 2017.

[20] C. Nadeau and A. Krupa, "Intensity-Based Ultrasound Visual Servoing: Modeling and Validation With 2-D and 3-D Probes," *IEEE Transactions on Robotics*, vol. 29, no. 4, pp. 1003–1015, aug 2013.

[21] P. Abolmaesumi, S. Salcudean, Wen-Hong Zhu, M. Sirouspour, and S. DiMaio, "Image-guided control of a robot for medical ultrasound," *IEEE Transactions on Robotics and Automation*, vol. 18, no. 1, pp. 11–23, 2002.

[22] R. Mebarki, A. Krupa, and F. Chaumette, "2-D Ultrasound Probe Complete Guidance by Visual Servoing Using Image Moments," *IEEE Transactions on Robotics*, vol. 26, no. 2, pp. 296–306, apr 2010.

[23] A. Krupa, G. Fichtinger, and G. D. Hager, "Real-time Motion Stabilization with B-mode Ultrasound Using Image Speckle Information and Visual Servoing," *The International Journal of Robotics Research*, vol. 28, no. 10, pp. 1334–1354, oct 2009.

[24] R. Nakadate, J. Solis, A. Takanishi, E. Minagawa, M. Sugawara, and K. Niki, "Out-of-plane visual servoing method for tracking the carotid artery with a robot-assisted ultrasound diagnostic system," in *2011 IEEE International Conference on Robotics and Automation*. IEEE, may 2011, pp. 5267–5272.

[25] O. Khatib, "A Unified approach The operational space formulation.pdf," pp. 43 – 53, 1987.

[26] A. Karamalis, W. Wein, T. Klein, and N. Navab, "Ultrasound confidence maps using random walks," *Medical Image Analysis*, vol. 16, no. 6, pp. 1101–1112, aug 2012.

[27] N. Chernov, "C++ code for circle fitting algorithms."

[28] G. Schreiber, A. Stemmer, and R. Bischoff, "The fast research interface for the kuka lightweight robot," *IEEE Workshop on Innovative Robot Control Architectures for Demanding (Research) Applications How to Modify and Enhance Commercial Controllers (ICRA 2010)*, pp. 15–21, 2010.

[29] A. Gefen and B. Dilmoney, "Mechanics of the normal woman's breast," *Technology and Health Care*, vol. 15, no. 4, pp. 259–271, jul 2007.

[30] A. Samani, J. Zubovits, and D. Plewes, "Elastic moduli of normal and pathological human breast tissues: An inversion-technique-based investigation of 169 samples," *Physics in Medicine and Biology*, vol. 52, no. 6, pp. 1565–1576, 2007.

[31] W. Li, B. Belmont, and A. Shih, "Design and Manufacture of Polyvinyl Chloride (PVC) Tissue Mimicking Material for Needle Insertion," *Procedia Manufacturing*, vol. 1, pp. 866–878, 2015.